







# Proteomics and phosphoproteomics of failing human left ventricle identifies dilated cardiomyopathy-associated phosphorylation of CTNNA3

Cristine J. Reitz<sup>a,b</sup> , Marjan Tavassoli<sup>a,b</sup>, Da Hye Kim<sup>a,b</sup>, Saumya Shah<sup>c</sup>, Robert Lakin<sup>d</sup>, Allen C. T. Teng<sup>a,b</sup>, Yu-Qing Zhou<sup>b</sup>, Wenping Li<sup>a,b</sup>, Sina Hadipour-Lakmehsari<sup>a,b</sup>, Peter H. Backx<sup>d</sup>, Andrew Emill<sup>e,f,g</sup>, Gavin Y. Oudit<sup>c,h,1</sup> , Uros Kuzmanov<sup>a,b,1</sup> , and Anthony O. Gramolini<sup>a,b,1</sup> 

Edited by Steven O. Marx, Columbia University Irving Medical Center, New York, NY; received July 15, 2022; accepted March 24, 2023  
by Editorial Board Member Andrew R. Marks

The prognosis and treatment outcomes of heart failure (HF) patients rely heavily on disease etiology, yet the majority of underlying signaling mechanisms are complex and not fully elucidated. Phosphorylation is a major point of protein regulation with rapid and profound effects on the function and activity of protein networks. Currently, there is a lack of comprehensive proteomic and phosphoproteomic studies examining cardiac tissue from HF patients with either dilated dilated cardiomyopathy (DCM) or ischemic cardiomyopathy (ICM). Here, we used a combined proteomic and phosphoproteomic approach to identify and quantify more than 5,000 total proteins with greater than 13,000 corresponding phosphorylation sites across explanted left ventricle (LV) tissue samples, including HF patients with DCM vs. nonfailing controls (NFC), and left ventricular infarct vs. noninfarct, and periinfarct vs. noninfarct regions of HF patients with ICM. Each pair-wise comparison revealed unique global proteomic and phosphoproteomic profiles with both shared and etiology-specific perturbations. With this approach, we identified a DCM-associated hyperphosphorylation cluster in the cardiomyocyte intercalated disc (ICD) protein,  $\alpha$ T-catenin (CTNNA3). We demonstrate using both ex vivo isolated cardiomyocytes and in vivo using an AAV9-mediated overexpression mouse model, that CTNNA3 phosphorylation at these residues plays a key role in maintaining protein localization at the cardiomyocyte ICD to regulate conductance and cell–cell adhesion. Collectively, this integrative proteomic/phosphoproteomic approach identifies region- and etiology-associated signaling pathways in human HF and describes a role for CTNNA3 phosphorylation in the pathophysiology of DCM.

heart failure | phosphoproteomics | signaling | bioinformatics | intercalated disc

Heart failure (HF) is clinically defined as the inability of the heart to maintain sufficient systemic circulation. Despite considerable efforts to improve prognosis and treatment, increasing incidence and 5-y mortality rate for HF patients remain high (1), highlighting a need for a deeper understanding of underlying disease mechanisms and limitations of current clinical interventions (2–4).

HF patients are managed based on clinical symptoms but disease etiology remains a key determinant of clinical prognosis and treatment outcomes (5–7). Ischemic cardiomyopathy (ICM) and dilated cardiomyopathy (DCM) are two of the most common causes of HF (1). Patients with DCM present with ventricular dilatation and impaired systolic function whereas the initial ischemic insult in ICM patients results in cellular apoptosis and loss of contractile function within the infarct followed by secondary cellular remodeling events (8, 9). Pathological cardiac remodeling disrupts various aspects of normal myocardial structure and function leading to inflammation, fibrosis, altered metabolism and myocardial contractility, and electrical disturbances. Thus, the delineation of perturbed signaling pathways of these two HF etiologies is of paramount importance for the clinical development of diagnostic and therapeutic strategies.

Numerous signaling cascades have been extensively studied in experimental cardiovascular disease models and in patients with ICM and DCM, in an attempt to discover key protein or pathway targets that may reverse or prevent further deterioration in cardiac function (10–14). Phosphorylation is a key dynamic modulator of signaling to rapidly and precisely drive the activation, localization, and degradation of proteins. In the setting of cardiac pathology, phosphorylation of key cardiac proteins, such as ryanodine receptor 2, titin, troponin I, phospholamban, and others, is known to integrate signaling cascades and regulate myocardial stiffening, contractility, and calcium cycling rates to both shape and respond to pathological stimuli (15–18). Harnessing the high-throughput power of

## Significance

Despite the profound effects of posttranslational protein modifications on downstream signaling events, limited studies have investigated the cardiac phosphoproteome in the context of human heart failure (HF). Here, we characterize differential regulation of major signaling networks along with upstream receptors and downstream effectors in HF patients with dilated cardiomyopathy (DCM) or ischemic cardiomyopathy (ICM).  $\alpha$ T-catenin phosphorylation was identified as a DCM-associated mechanism regulating cardiac structure and function, cardiomyocyte intercalated disc (ICD) organization, and protein–protein interactions at the adherens junction/area composita, using both ex vivo and in vivo experimental models. This work emphasizes the utility of our integrative analyses of proteome and phosphoproteome from patient ventricular samples to further our understanding of the etiology- and region-specific mechanisms underlying HF progression.

The authors declare no competing interest.

This article is a PNAS Direct Submission. S.O.M. is a guest editor invited by the Editorial Board.

Copyright © 2023 the Author(s). Published by PNAS. This article is distributed under Creative Commons Attribution-NonCommercial-NoDerivatives License 4.0 (CC BY-NC-ND).

<sup>1</sup>To whom correspondence may be addressed. Email: gavin.oudit@ualberta.ca, uros.kuzmanov@utoronto.ca, or anthony.gramolini@utoronto.ca.

This article contains supporting information online at <https://www.pnas.org/lookup/suppl/doi:10.1073/pnas.2212118120/-DCSupplemental>.

Published May 1, 2023.

mass spectrometry-driven phosphoproteomics has been essential to discovering the wide-spread presence of phosphorylation and its functional roles in the complex signaling interplay in failing hearts.

The present study provides an in-depth, integrative proteomic and phosphoproteomic analysis of perturbed myocardial molecular signatures between HF patients suffering from DCM and ICM. Myocardial tissue explants from the left ventricle (LV) infarct, periinfarct, and noninfarct regions of HF patients with ICM, the LV of HF patients with DCM, and the LV of nonfailing controls (NFC) were labeled with 10-plex tandem mass tags (TMT) and subjected to liquid chromatography–tandem mass spectrometry (LC-MS/MS) proteomic and phosphoproteomic analyses. Following stringent computational and bioinformatic analyses, dozens of disrupted molecular networks were found in dilated and post-MI failing LV. Ranking of functionally enriched pathways and phosphoprotein candidates revealed myocyte adhesion and phosphorylation of the intercalated disc (ICD) protein,  $\alpha$ T-catenin (CTNNA3), respectively, as uniquely up-regulated in DCM hearts. Using ex vivo characterization in isolated adult mouse cardiomyocytes as well as generation of an in vivo AAV9-mediated overexpression mouse model, we demonstrate a role for CTNNA3 phosphorylation in regulating ICD organization, conductance, and cell–cell adhesion. Collectively, these comprehensive discovery datasets of etiology- and region-associated signaling pathways in both DCM and ICM are clinically relevant and should be further explored for their therapeutic and diagnostic potential.

## Results

**Patient and Sample Characteristics.** Left ventricular anterior wall tissue explants were collected from three groups of patients and utilized for downstream proteomic and phosphoproteomic profiling: i) DCM patients with failing hearts; ii) ICM patients with failing hearts resulting from MI; and iii) nonfailing control (NFC) samples from donors with no history of heart disease that were unsuitable for transplant (Fig. 1 and Table 1). Patient clinical characteristics are listed in Table 1. No vasopressor or inotropes were used in the DCM or ICM patients immediately prior to heart transplantation. All four NFC patients received intravenous vasopressin and norepinephrine as standard pressor and inotropic support. Three different samples from the left ventricular wall were collected from each patient in the ICM group: infarct (INF), periinfarct (PERI), and noninfarcted (NI) regions. Trichrome and picrosirius red (PSR) staining demonstrated increased myocardial fibrosis in tissue from DCM patients and the periinfarct region of ICM patients when compared to NFC, with greater fibrosis seen in the DCM group (SI Appendix, Fig. S1). Immunofluorescent staining with wheat germ agglutinin (WGA) revealed increased cardiomyocyte cross-sectional area in the periinfarct and DCM samples, consistent with pathological hypertrophy (SI Appendix, Fig. S1). These results reveal the pathological remodeling in these explanted failing human hearts.

### Overview of Global Proteomic and Phosphoproteomic Analyses.

Left ventricular samples isolated from DCM and NFC patients and left ventricular samples isolated from infarct, periinfarct, and noninfarct regions from ICM patients were subjected to LC-MS/MS for an in-depth characterization of globally expressed proteins and phosphoproteins (Fig. 1 and SI Appendix, Table S1). Across the three pairwise comparisons (DCM vs. NFC; infarct vs. noninfarct in ICM; periinfarct vs. noninfarct in ICM), a total of 3,738 proteins and 13,624 phosphorylation sites corresponding to 3,240 phosphoproteins were identified from left ventricular tissues,

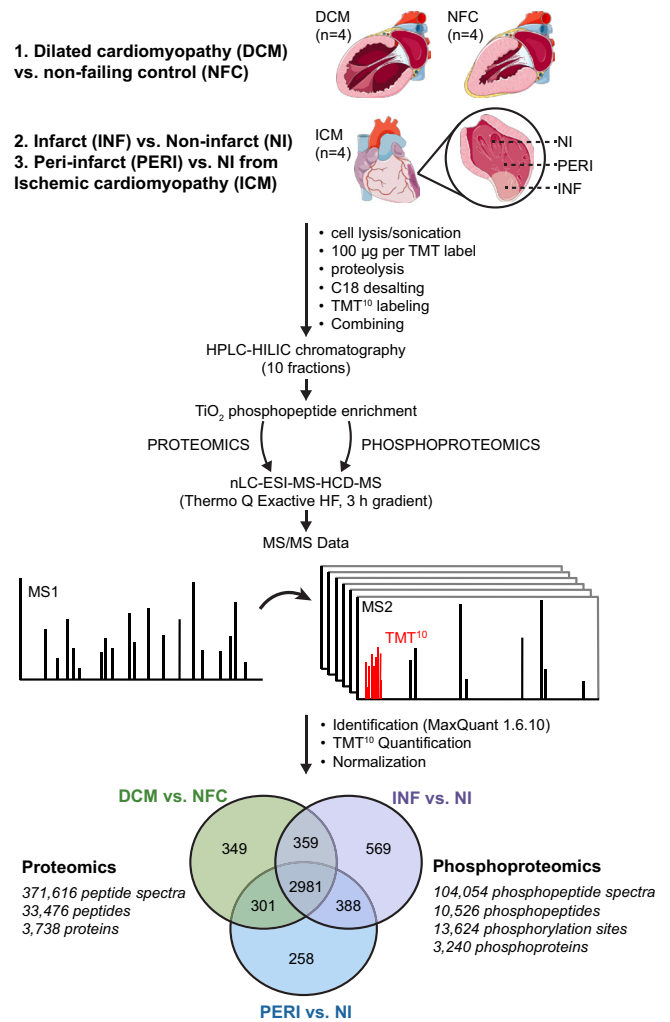


**Fig. 1.** Overview of experimental workflow with a summary of proteomic and phosphoproteomic data with assigned PSMs and proteins identified. Left ventricular tissues from DCM patients with failing hearts vs. NFC and from infarct, periinfarct, and noninfarct regions sampled from each ICM patient with failing hearts were processed for LC-MS/MS and tagged with 10-plex TMT for relative quantification. Venn diagram depicts all identified proteins and phosphoproteins from each pairwise comparison.

totaling 5,570 unique proteins (Fig. 1). Global distribution data and raw datasets of proteins and phosphorylation sites are shown in SI Appendix, Fig. S2, and Datasets S1 and S2, respectively. The differences in the number of proteins/phosphorylation sites altered within each comparison (Fig. 2 A and B) are reflected in the distinct clustering of DCM and infarct samples from their controls, NFC and noninfarct, respectively, by 2D principal component analysis (PCA) (Fig. 2 A and B and SI Appendix, Fig. S3). In contrast to the infarct vs. noninfarct comparison, the number of altered proteins and phosphorylation sites between periinfarct and noninfarcted samples of the ventricular myocardium were noticeably lower, with 241 altered proteins and phosphorylation sites, supported by a shorter minimum distance between the two sample groups in the PCA analysis (Fig. 2C). Despite the limited sample size of patients, our multiplexed study design allowed for in-depth coverage of the global cardiac proteome in HF. In order to assess our data in the context of larger, diverse patient samples, we performed integrative analysis with 3 recent open-source datasets: Li et al. (global LV proteomics (19);  $n = 15$  DCM,  $n = 15$  ICM,  $n = 15$  NFC), Tomin et al. (global LV proteomics (20);  $n = 3$  DCM,  $n = 12$  ICM,  $n = 10$  NFC), and Reichart et al. (LV single-cell transcriptomics (21);  $n = 61$  DCM,  $n = 18$  NFC).

**Table 1. Clinical characteristics of patient tissues**

Etiology	DCM				ICM				NFC				
Patient Code	DCM1	DCM2	DCM3	DCM4	INF1/PERI1	INF2/PERI2	INF3/PERI3	INF4/PERI4	NFC1	NFC2	NFC3	NFC4	
Sex	M	M	F	F	M	M	F	F	F	F	M	M	
Age at transplant (years)	51	45	55	62	55	62	57	51	21	42	38	54	
Medications (1 = yes; 0 = no)													
Patient code	LVAD	EF (%)	LV mass (g/m <sup>2</sup> )	LVIDd (cm)	LVIDs (cm)	LVPWd (cm)	Duration HF (months)	Hb (g/L)	eGFR (mL/min/1.73 m <sup>2</sup> )	ACEi/ARB	Beta-blocker	MRA	Vasopressor
DCM1	No	15	155.9	6.6	5.6	1.1	60	122	71	1	1	1	0
DCM2	No	25	122.6	6.3	6.0	1.0	75	134	63	1	0	1	0
DCM3	No	29	112.3	5.1	4.9	1.2	81	131	79	1	1	0	0
DCM4	No	20	146.7	6.2	5.3	1.2	66	118	58	1	1	1	0
INF1/PERI1	Yes	22	127.0 / 50.1	5.3 / 4.1	4.5 / 3.5	0.9 / 0.5	73	129	59	1	1	1	0
INF2/PERI2	Yes	24	- / 85.3	- / 5.5	- / 4.6	- / 0.7	64	130	54	1	1	1	0
INF3/PERI3	Yes	31	153.6 / 126.4	5.1 / 5.1	4.6 / 3.9	1.3 / 1.2	84	116	62	1	1	0	0
INF4/PERI4	Yes	19	- / 84.6	- / 5.0	- / 4.1	- / 1.0	58	123	73	1	1	1	0

Abbreviations: DCM, dilated cardiomyopathy; ICM, ischemic cardiomyopathy; INF, infarct; PERI, periinfarct; NFC, nonfailing control; M, male; F, female; LVAD, left ventricular assist device; EF, ejection fraction; LV mass, left ventricular mass; LVIDd, left ventricular internal dimension at diastole; LVIDs, left ventricular internal dimension at systole; LVPWd, left ventricular posterior wall at end diastole; HF, heart failure; Hb, hemoglobin; eGFR, estimated glomerular filtration rate; ACEi/ARB, angiotensin-converting enzyme inhibitor/angiotensin receptor blocker; MRA, mineralocorticoid receptor antagonist. ICM data are shown as pre/post-LVAD for LV mass, LVIDd, LVIDs, and LVPWd; EF data are pre-LVAD. NFC heart samples were procured through the HOPE (Human Organ Procurement and Exchange) program from donors with no history of cardiac disease that were unsuitable for transplant.

Integrative analyses across the datasets showed a high degree of total protein coverage overlap from these studies in our dataset (85% of proteins from Li et al.; 98% of proteins from Tomin et al.; >1,300 additional proteins identified only in our dataset) as well as strong correlation at the pathway level for both DCM ( $r = 0.95$ ) and ICM ( $r = 0.97$ ) annotations (*SI Appendix, Fig. S4*), with discrepancies in differential protein/gene expression likely largely attributable to inter-patient variability, variability in sample collection time at transplant/autopsy, and collection methodology across different research centers, as well as established discordance between RNA and protein levels across human tissues (22).

The representative cardiac proteome and phosphoproteome coverage in all three of our datasets, encompassing all protein and phosphoprotein identifications, were then characterized according to Reactome pathways, Gene Ontology Biological Process (GOBP), Cellular Component (GOCC), and Molecular Function (GOMF) (Fig. 2D). (Phospho)protein identifications of each dataset were then independently analyzed for over-represented gene annotations to identify converging and differential pathway enrichment between the DCM, infarct, and periinfarct samples, as compared to their respective controls (Fig. 2E and *Dataset S3*). Gene annotations at all classifications and the magnitude of overrepresentation relative to the total human proteome were highly overlapped between the three individual datasets, as shown in the Venn diagrams in Fig. 2E.

**Major Individual Protein and Phosphorylation Site Disturbances in ICM and DCM.** Proteomic analysis revealed 757 and 544 proteins to be altered (two-tailed Student's *t* test,  $P$ -value < 0.05) in DCM and infarct compared to their controls, NFC and noninfarct, respectively, 137 of which were modified in both pathologies (Figs. 2A and B and 3A). Corresponding phosphoproteomic profiling revealed 1,435 altered phosphorylation sites in DCM and 3,107 in infarct with an overlap of 522 phosphorylation sites,

which corresponded to 625 phosphoproteins in DCM and 1,239 in infarct with an overlap of 430 phosphoproteins (Figs. 2A and B and 3A). For the purpose of a direct comparison between ICM and DCM, protein and phosphorylation site expression levels of commonly identified components between DCM and INF (when compared against the relevant controls) were visualized (Fig. 3B and *Dataset S1*). Interestingly, proteomic data showed a selective down-regulation of contractile proteins (TTN, TCAP, NEBL, MYH7, and MYBPC3) as well as cell adhesion proteins (DSG2, DSP, and CTNNA1) in DCM in contrast to their stable expression in infarcted tissue (Fig. 3B, *SI Appendix, Fig. S5A*, and *Dataset S1*). Kinase networks that regulate the DCM and infarct phosphoproteome were determined by associating each significantly ( $P$ -value < 0.05) altered phosphorylation site with a linear motif based on the identified surrounding sequence and was given potential kinases and/or binding partners using the “add linear motifs” function on Perseus (*Dataset S4*). The 10 most abundant motifs identified in DCM and infarct were identical regarding its order and frequency (Fig. 3C), suggesting that these kinases play a central role in intracellular cardiac signaling regardless of disease etiology.

**Detailed Protein and Phosphorylation Site Level Annotation of Central Signaling Mechanisms in HF.** For subsequent bioinformatic analyses, the proteome and phosphoproteome were merged to have each protein represented once in the combined (phospho) proteome by either its expression or phosphorylation site intensity values (Fig. 3D). This approach yielded one dataset for each etiology, DCM and infarct, and retained the most significantly altered identifications at protein or phosphorylation site level for all (phospho)proteins identified. Significantly ( $P$ -value < 0.05) up-regulated and down-regulated (phospho)proteins from DCM and infarct were independently analyzed, i.e., four separate analyses, for enriched gene annotations to compare protein coverage and

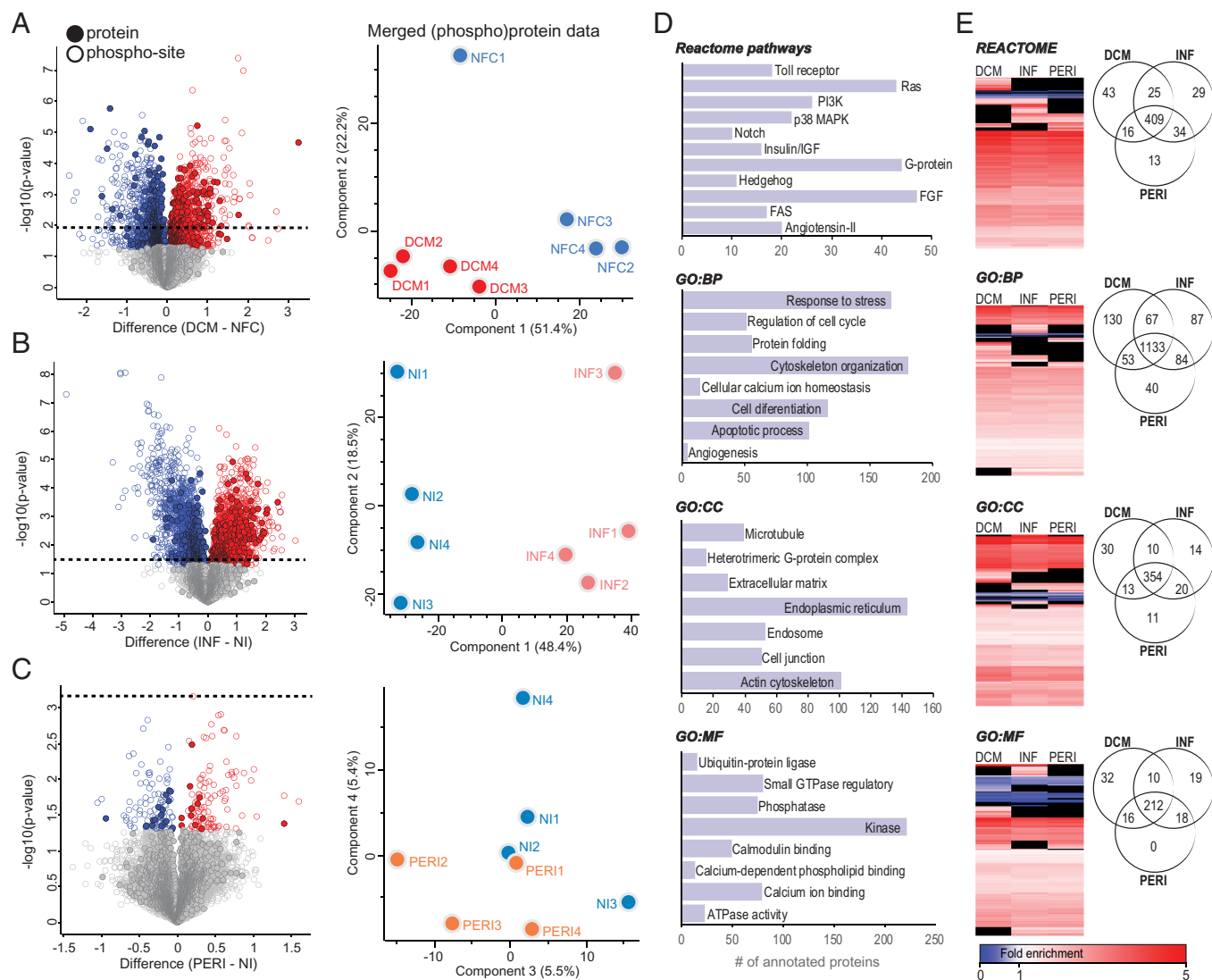


**Fig. 2.** Perturbed proteome and phosphoproteome in DCM patients and its region-specific manifestation in ICM patients. (A–C) Volcano and principal component analysis plots of the different etiology pairwise comparisons (A, DCM vs. NFC; B, infarct vs. noninfarct in ICM; C, periinfarct vs. noninfarct in ICM). Volcano plots show log-transformed values of proteins (closed circles) and phosphorylation sites (open circles) with differential expression (Student's *t* test,  $P < 0.05$ ) between each pairwise comparison of pathological samples and related controls. Proteins/phosphorylation sites up- or down-regulated in pathology were colored red or blue, respectively. Broken lines in volcano plots represent a further permutation-based corrected *P*-value significance level ( $q < 0.05$ ). Principal component analysis plots showed distinct clustering of patient sample groups resulting from merged protein and phosphorylation site quantitative information. (D) Overview of selected cardiac-relevant gene annotation distributions in the failing human LV from all (phospho)protein identifications found in at least one of the three pairwise datasets (DCM vs. NFC, infarct vs. noninfarct, and periinfarct vs. noninfarct). GO = gene ontology, BP = biological process, CC = cellular component, MF = molecular function. (E) Global view of hierarchical clustering and coverage comparisons of significantly ( $q\text{-value} < 0.05$ ) over-represented gene annotations between each dataset.

identify broad patterns that may determine which proteins are up- or down-regulated (Fig. 3E, SI Appendix, Fig. S5B, and Dataset S5). HF-associated processes including regulation of PTEN and focal adhesion were significantly (Fisher's exact overrepresentation test,  $q\text{-value} < 0.05$ ) enriched among up-regulated (phospho)proteins in both DCM and infarct (23, 24). Moreover, gene set enrichment analysis resulted in 560 gene sets significantly ( $q\text{-value} < 0.05$ ) enriched in DCM compared to NFC and 743 gene sets in the infarct compared to noninfarct. DCM and infarct datasets shared 357 gene sets that were significantly enriched in both ICM and DCM samples, leaving 203 and 386 gene sets uniquely associated with DCM and INF, respectively (SI Appendix, Figs. S6 and S7 and Dataset S6). Collectively, these pathways were annotated with relevant quantitative information from the (phospho)proteomic profiling of DCM and ICM samples compared against their relevant controls (SI Appendix, Fig. S8), providing an illustrated overview of the major signaling pathways altered in HF in our datasets.

### Functional Enrichment Analyses Identify Cell-Cell Adhesion Pathways in DCM.

Ranking of gene ontology data (Dataset S5) demonstrated the top 10 significantly enriched ( $P < 0.05$ ) biological processes, cellular components, and molecular functions in the DCM hearts (Fig. 3F). Interestingly, the highest enriched pathways up-regulated in DCM corresponded to myocyte adhesion, cell cortex/fascia adherens, and cell adhesive protein binding. In cardiac tissue, structural cell–cell adhesion and electrical and mechanical coupling between neighboring muscle cells is mediated by a highly specialized ICD region (25). Enriched annotations with functional relevance to the ICD cellular compartment identified corresponding molecular pathways of  $\alpha$ -catenin binding,  $\beta$ -catenin binding, and cadherin binding (SI Appendix, Fig. S9). At the proteome level, minor differences were observed in ICD protein abundance (Fig. 3G), yet over  $\frac{3}{4}$  of ICD proteins (10/13 proteins from this ICD cassette) showed significant ( $P < 0.05$ ) changes in phosphorylation levels in DCM

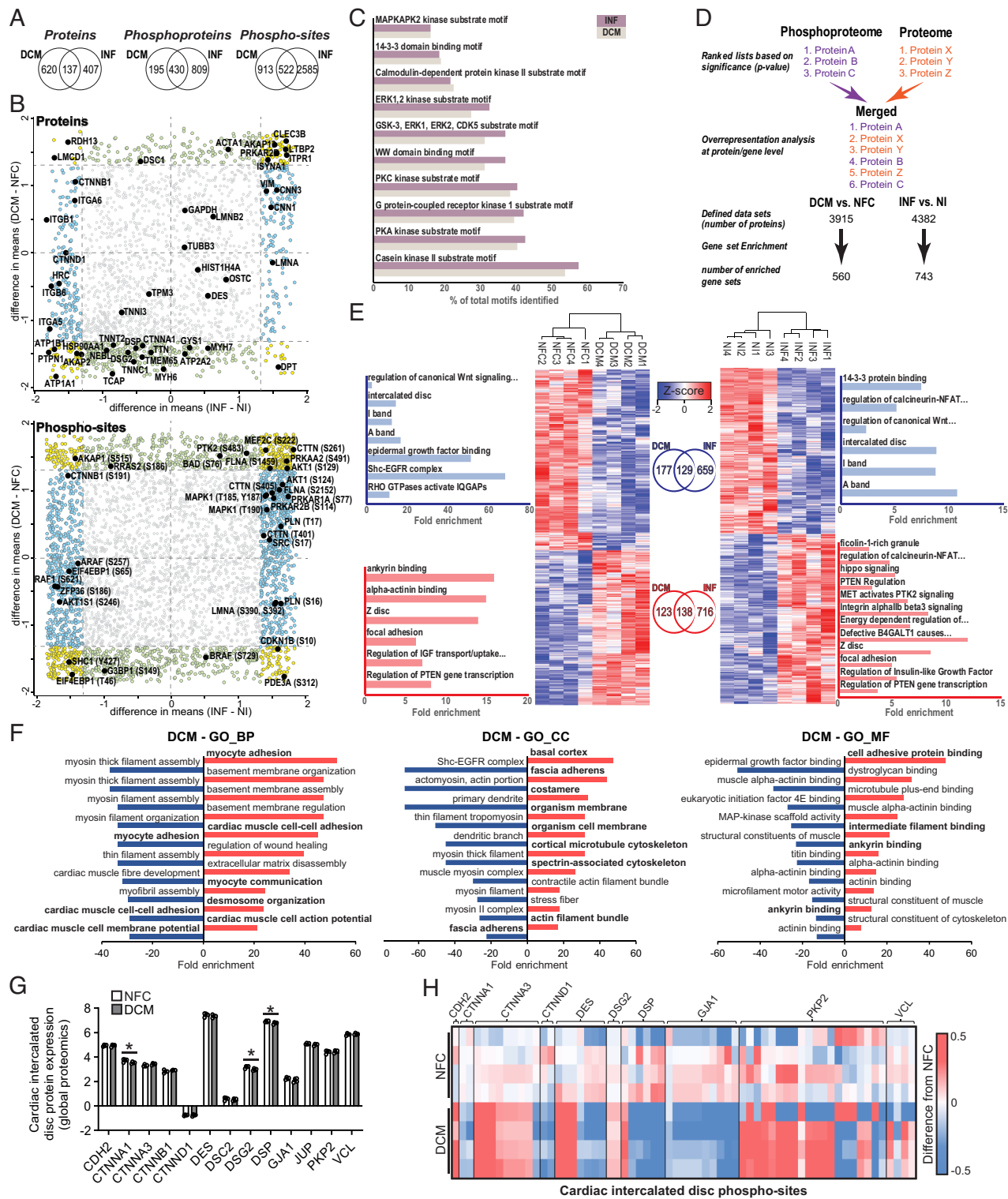


**Fig. 3.** Significantly altered protein expression and phosphorylation variance in HF according to patient disease. (A) Values denoting significantly ( $P$ -value  $< 0.05$ ) altered proteins, phosphoproteins, and phosphorylation sites in DCM and infarct and Venn diagrams representing the overlap. (B) Differential expression and quantification of commonly identified proteins and phosphorylation sites, respectively, in DCM and infarct by visualizing the difference in means (against controls) of z-scored protein or phosphorylation site intensity values with its significance ( $P$ -value  $< 0.05$ ) denoted in different colors: yellow (significantly altered in both DCM and INF), light blue (significantly altered in INF alone), and light green (significantly altered in DCM alone). Zoomed panels provided in *SI Appendix*. (C) Bioinformatics analysis of potential kinases and/or binding partners based on the surrounding sequence of altered phosphorylation sites revealed the 10 most common kinase and/or binding partner substrate motifs detected among significant phosphoproteins in DCM and infarct. (D) Workflow combining the phosphoproteomes and proteomes to yield a merged DCM (phospho)proteome and infarct (phospho)proteome for subsequent gene annotation overrepresentation and gene set enrichment analyses. (E) Hierarchical clustering of z-score normalized intensities of proteins and phosphorylation sites with comparisons of gene sets significantly ( $q$ -value  $< 0.05$ ) enriched in up-regulated proteins (in red) and down-regulated proteins (in blue) in DCM and infarct. Zoomed panels provided in *SI Appendix*. (F) Top 10 significantly ( $P < 0.05$ ) enriched gene ontology (GO) biological processes (Left), cellular components (Middle), and molecular functions (Right), following analysis of enriched gene annotations in DCM as compared to NFC. Top enriched pathways related to cardiac muscle cell-cell adhesion (in bold). (G) Cardiac muscle cell ICD normalized protein expression in DCM vs. NFC from proteomic data,  $*P < 0.05$ . (H) Heat map of cardiac ICD protein phosphosites up-regulated (in red) and down-regulated (in blue) in DCM vs. NFC. Hierarchical clustering of these phosphosites is provided in *SI Appendix*.

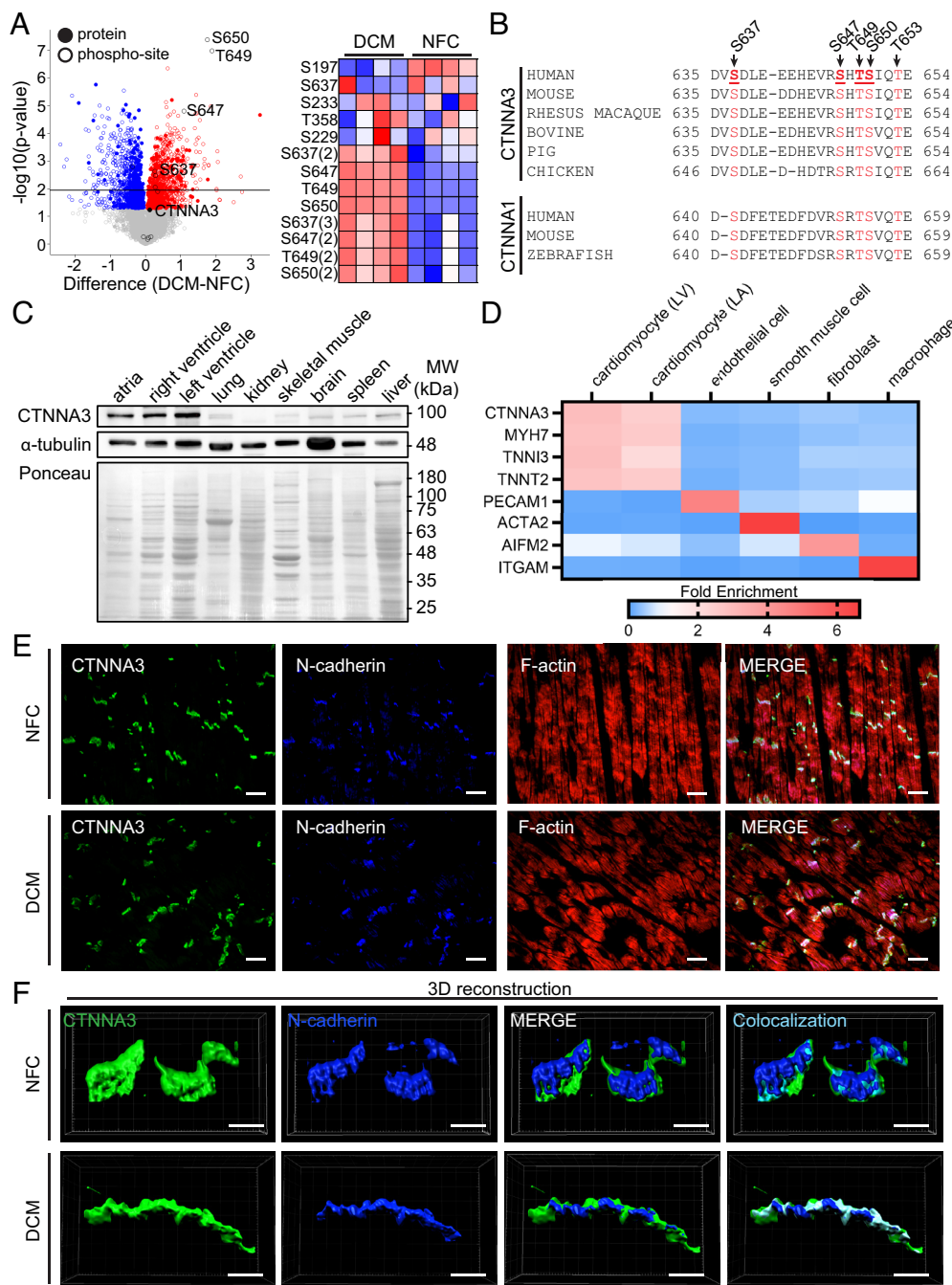


**Fig. 4.** Cardiomyocyte-enriched ICD protein, CTNNA3, is hyperphosphorylated in DCM. (A) Log-transformed *P*-values of proteins (closed circles) and phosphorylation sites (open circles) up-regulated (red) or down-regulated (blue) in DCM vs. NFC, with CTNNA3 protein and phosphorylation sites designated in black (left; volcano plot is replotted from Fig. 2A), and heat map of CTNNA3 phosphosites (right; expanded view of data from Fig. 3H) with proteins/phosphorylation sites up- or down-regulated in DCM colored red or blue, respectively. Numbers in brackets [e.g., S637 (2)] designate separate peptides used to quantify a particular phosphorylation site, where in other additional phosphorylation sites were also present on the peptide. (B) Conservation of phosphosites across species between  $\alpha$ T-catenin (CTNNA3) and  $\alpha$ E-catenin (CTNNA1). Phosphosites are denoted in red, sites with significantly increased phosphorylation in human DCM hearts are bold and underlined. (C) Immunoblot analysis of CTNNA3 expression across mouse tissues demonstrated cardiac-enriched expression. (D) Analysis of an open-access single-cell RNA-seq dataset (GEO accession: GSE109816) from human heart tissue showed cardiac CTNNA3 expression is enriched in the cardiomyocyte. LV = left ventricle, LA = left atria. (E) Confocal imaging of CTNNA3, N-cadherin, and F-actin in human NFC and DCM heart tissue. (Scale bar, 20  $\mu$ m.) (F) Three-dimensional reconstruction of CTNNA3 and N-cadherin localization at the ICD in cardiac tissue from NFC and DCM patients. (Scale bar, 5  $\mu$ m.) Images are representative of *n*=3 independent biological replicates.

(either up- or down-regulated), as compared to NFC (Fig. 3H and SI Appendix, Fig. S10), suggesting that phosphorylation of ICD proteins comprises a major, yet previously uncharacterized, process underlying perturbed protein regulation and signaling in DCM. Interestingly, hierarchical clustering showed segregation between phosphorylation of proteins at the gap junction/desmosome as being down-regulated in DCM and phosphorylation of proteins at the adherens junction/area composita as being up-regulated in DCM (SI Appendix, Fig. S10). Two proteins from the ICD protein cassette, CTNNB1 and JUP, did not show significant phosphorylation differences despite detection of several phosphosites in the mass spectrometry data, while a third protein, DSC2, had no phosphosites detected in the DCM samples. Together, these data identify DCM-associated changes at the ICD and reinforce the utility of phosphoproteomic analyses to characterize pathways in HF pathophysiology.

**Hyperphosphorylation of the Cardiomyocyte-Enriched Protein,  $\alpha$ T-Catenin (CTNNA3), in DCM.** To identify previously uncharacterized phosphoprotein candidates preferentially altered in DCM, we applied a ranking strategy to all 625 differentially regulated phosphoproteins and identified CTNNA3 ( $\alpha$ T-catenin) with the highest ranked phosphorylation site *q*-value, and with no corresponding significant change recorded at the protein level in DCM, as compared to NFC (Fig. 4A). Of 8 unique phosphorylation sites identified in the CTNNA3 protein, five showed significant up regulation or downregulation in DCM (Fig. 4A). Interestingly, we detected four hyperphosphorylated residues in DCM: S637, S647, T649, and S650, by mass spectrometry, all clustered within a span of 14 amino acids (Fig. 4A and B). These changes appeared to be specific to DCM, with no significant differences in phosphorylation status observed at these loci in the ICM samples. Kinase motif enrichment identified the top up- and down-regulated motifs in DCM, with CKI, GSK,

ERKs, CDK5, PKC $\epsilon$ , and WW domain as the putative kinases and binding motifs for the phosphoresidues identified in the CTNNA3 protein (*SI Appendix, Fig. S11*). As our identified phosphosites are located within a conserved amino acid region, previously termed the “phospho (P)-linker” domain (26), we used the ClinVar database to identify variants within this domain, between amino acids 627 to 660 of the CTNNA3 protein. This analysis revealed 60 assertions for variants at 37 sites within the CTNNA3 gene, all with varying clinical association to arrhythmogenic right ventricular cardiomyopathy, including a single-nucleotide variant at one of our putative phosphosites, S650 (*SI Appendix, Fig. S12 and Table S2*).

CTNNA3 is a member of the  $\alpha$ -catenin protein family, which show robust species conservation across mammalian taxa, with divergent clustering of the cardiac muscle-enriched CTNNA3, by phylogeny and human protein atlas analysis (*SI Appendix, Fig. S13*). A sequence alignment demonstrated that this region is highly conserved across species and  $\alpha$ -catenin isoforms (Fig. 4*B*), which identified an additional putative phosphorylation site at T653 (26). CTNNA3 is highly enriched in mouse atria and ventricular tissue (Fig. 4*C* and *SI Appendix, Fig. S14*), and this enrichment appears specific to the cardiomyocyte (Fig. 4*D*), based on open-access human heart single-cell RNA-seq (27). Together, these data support the notion of an evolutionarily conserved phosphodomain in the cardiomyocyte-enriched protein CTNNA3.

#### Microscopy Analysis of CTNNA3 at the ICD in Human DCM Hearts.

We then performed confocal imaging of human heart LV tissue sections from DCM and NFC patients and localized CTNNA3 to the cardiomyocyte ICD region with a high degree of colocalization with the ICD marker, N-cadherin (Fig. 4*E*). A similar staining pattern was observed in mouse cardiac tissue (*SI Appendix, Fig. S15A*) and in isolated adult mouse cardiomyocytes (*SI Appendix, Fig. S15B–E*). Higher magnification imaging in human LV tissue (*SI Appendix, Fig. S15F*), coupled with 3-dimensional reconstruction analysis (Fig. 4*F*), demonstrated reorganization of the ICD structure in DCM hearts. DCM tissues showed ICD lengthening ( $17.20 \pm 1.87 \mu\text{m}$  vs.  $10.07 \pm 0.76 \mu\text{m}$ ;  $P < 0.05$ ) and reduced ICD thickness ( $1.88 \pm 0.12 \mu\text{m}$  vs.  $3.27 \pm 0.12 \mu\text{m}$ ;  $P < 0.005$ ), as compared to NFC, consistent with previous reports of ICD remodeling in DCM (28). Interestingly, colocalization analyses revealed increased CTNNA3 and N-cadherin colocalization in the DCM hearts (Pearson’s correlation coefficient;  $0.71 \pm 0.02$  vs.  $0.55 \pm 0.04$ ;  $P < 0.05$ ), as compared to NFC (Fig. 4*F*). As phosphorylation can influence protein–protein interactions, there exists the possibility that altered phosphorylation status of CTNNA3 may play a role in protein localization and interaction with N-cadherin at the ICD.

#### Functional Characterization of CTNNA3 Phosphorylation in Cardiomyocytes.

To determine the contribution of phosphorylation at the identified amino acid residues (Fig. 4*B*) to CTNNA3 function, we generated FLAG-tagged human CTNNA3 constructs with wild-type [ $\alpha$ T-cat wild type (WT)], nonphosphorylatable ( $\alpha$ T-cat 5A), and phosphomimetic ( $\alpha$ T-cat 5D) forms (Fig. 5*A*). To characterize the function of these constructs *ex vivo*, isolated adult mouse cardiomyocytes were transduced with lentiviral vectors harboring  $\alpha$ T-cat variants (WT, 5A, or 5D). Immunoblot analysis demonstrated an ~fourfold increase in CTNNA3 levels, with clear FLAG expression of all constructs (Fig. 5*B* and *SI Appendix, Fig. S16A and B*). Confocal imaging of transduced cells revealed the expected localization of  $\alpha$ T-catenin-WT-FLAG as well as  $\alpha$ T-catenin-5D-FLAG at the ICDs, whereas  $\alpha$ T-catenin-5A-FLAG showed internalized expression throughout the cell (Fig. 5*C–E* and *SI Appendix, Fig. S17A*). These data indicate that phosphorylation of CTNNA3 affects protein localization in isolated adult mouse cardiomyocytes.

To investigate whether mutant CTNNA3 overexpression alters ICD organization in the cardiomyocyte, we assessed ICD protein expression and localization in lentivirus transduced adult mouse cardiomyocytes. Immunoblot analyses showed no change in overall expression of N-cadherin, connexin 43, plakophilin 2,  $\beta$ -catenin, and vinculin, in the transduced myocytes (*SI Appendix, Fig. S16C*); however, confocal imaging revealed increased internalized N-cadherin signal in 5A phosphonull cardiomyocytes (Fig. 5*F–G* and *SI Appendix, Fig. S17B*), as compared to WT and 5D cells. We next assessed whether disruption of N-cadherin in the 5A cells leads to impaired cell–cell adhesion. HEK-293T cells were transfected with WT, 5A, or 5D constructs, and cell monolayers subjected to a fragmentation assay. We found a higher number of cell fragments in 5A-transfected cells, as compared to all other groups (Fig. 5*H*), indicative of weaker cell–cell adhesion in the absence of CTNNA3 phosphorylation.

#### Overexpression of Phosphonull CTNNA3 Leads to Cardiac Dysfunction and Conduction Defects *in vivo*.

In order to assess the effects of CTNNA3 phosphorylation in the intact myocardium, we created a mouse model of CTNNA3 phosphoconstruct overexpression by injecting mouse neonates (day 7 postbirth) with rAAV9-CTNNA3-WT, rAAV9-CTNNA3-5A, or empty rAAV9 control, and followed animals for up to 12 wk postinjection (Fig. 6*A*). Mice overexpressing phosphonull CTNNA3-5A protein showed reduced left ventricular contractile function as early as 4 wk postinjection, with increased left ventricular dimensions and reduced ejection fraction and fractional shortening, as compared to AAV9-empty and AAV9-CTNNA3-WT mice (Fig. 6*B* and Table 2). Overexpression of the phosphomimetic rAAV9-CTNNA3-5D did not alter cardiac function vs. control mice (data not shown). Cardiac electrical abnormalities were also observed in the CTNNA3-5A mice, with prolonged QTc interval compared to AAV9-empty, determined by noninvasive, conscious ECG recordings at 12 wk post-AAV9 injection (*SI Appendix, Table S3*). Mice were also subjected to  $\beta$ -adrenergic stimulation prior to ECG recording to assess arrhythmia susceptibility. Following acute isoproterenol administration, CTNNA3-5A mice showed a higher incidence of premature ventricular contractions (PVCs) (92.31% of CTNNA3-5A, 33.33% of empty, 53.85% of CTNNA3-WT mice) as well as a higher frequency of PVC occurrences per animal ( $10.08 \pm 3.09$  PVCs/mouse in CTNNA3-5A,  $1.44 \pm 0.77$  in empty,  $1.77 \pm 0.67$  in CTNNA3-WT) over 30 min of recording immediately postisoproterenol bolus (Fig. 6*C*). Given these changes in cardiac electrophysiology, we then assessed cardiac conduction using whole heart optical mapping. When isolated hearts were paced at 11 Hz, conductance across the left ventricular free wall showed reduced conduction velocity in CTNNA3-5A hearts, as compared to all other groups (Fig. 6*D*). Moreover, action potential duration (ADP<sub>90</sub>) was prolonged in the CTNNA3-5A hearts (*SI Appendix, Table S4*), supporting the observed increase in QTc interval in these mice. Cardiac histopathology at 12 wk demonstrated a mild increase in interstitial fibrosis in the CTNNA3-5A hearts by Masson’s trichrome and picrosirius red staining, as compared to CTNNA3-WT (*SI Appendix, Fig. S18*). Together these findings demonstrate adverse left ventricular remodeling, contractile dysfunction, and electrical conduction defects in response to stress in mice with cardiac-directed overexpression of phosphonull CTNNA3.

#### *In vivo* Overexpression of Phosphonull CTNNA3 Leads to ICD Remodeling and Protein Internalization.

Given that we observed adverse cardiac remodeling in the CTNNA3-5A mice, we next assessed changes at the level of the ICD. To visualize

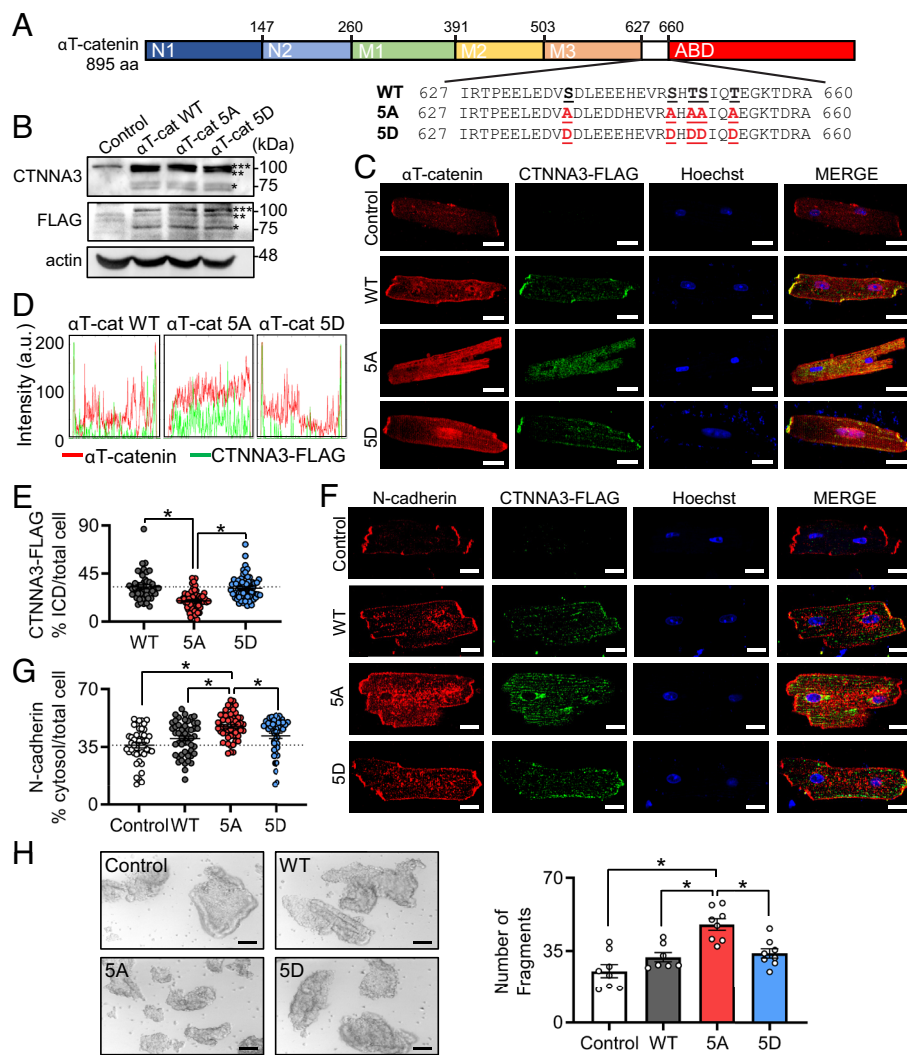


**Fig. 5.** CTNNA3 phosphorylation regulates cardiomyocyte ICD organization and cell-cell adhesion. (A) Schematic of CTNNA3 mutant constructs: WT, 5-site phosphonull (5A), and 5-site phosphomimetic (5D). (B) Immunoblot analysis of lentivirus-mediated overexpression of FLAG-tagged CTNNA3 constructs in adult mouse cardiomyocytes. Asterisks indicate three protein bands observed in overexpressing cells based on molecular weight analyses. (C) Confocal imaging of adult mouse cardiomyocytes stained with CTNNA3 and FLAG 48 h postlenticular transduction. (Scale bar, 20  $\mu$ m.) (D) Line scan analysis of confocal images in C demonstrated peak expression at the ICDs in WT and 5D, with internalized CTNNA3 expression in 5A cells. (E) Quantification of CTNNA3-FLAG localization at the cardiomyocyte ICD as a percent of the total cell intensity. (F) Confocal imaging of N-cadherin in adult mouse cardiomyocytes 48 h postlenticular transduction with CTNNA3-FLAG constructs showed (G) significant internalization of N-cadherin in 5A-expressing cells vs. control, WT, and 5D. (Scale bar, 20  $\mu$ m.) (H) Cell-cell adhesion assay by mechanical disruption. Brightfield images of cell fragments (Left) and quantification (Right), corresponding to the number of macroscopic fragments counted after shaking. (Scale bar, 100  $\mu$ m.) All images shown are representative of 40 to 60 cells captured per condition, from  $n = 3$  independent biological replicates.

CTNNA3 overexpression in the intact myocardium, we performed immunofluorescence imaging of cardiac tissue sections from mice at 12 wk post-AAV9 injection. We found significantly increased expression of both global  $\alpha$ T-catenin and FLAG-tagged CTNNA3 protein in both the AAV9-CTNNA3-WT and AAV9-CTNNA3-5A mice, but not in AAV9-empty controls, as expected (Fig. 6E and SI Appendix, Fig. S19A). Consistent with our observations in the lentiviral-transduced isolated cardiomyocytes, we observed a significant internalization of the CTNNA3-5A protein in the intact myocardium, with reduced proportion of the fluorescent signal at the ICD as compared to empty and CTNNA3-WT (Fig. 6E).

To determine whether changes in *in vivo* cardiac electrophysiology may be due to underlying gap junction remodeling, we performed confocal imaging of connexin 43 (Cx43), and found internalization/lateralization of the Cx43 signal along the length of the cardiomyocytes, along with reduced Cx43 colocalization with FLAG, in the CTNNA3-5A hearts (Fig. 6F and SI Appendix, Fig. S19B). Thus, loss of CTNNA3 phosphorylation led to gap junction dissociation from the adherens junction. Indeed, this gap junction dissociation has been well established in human and animal models of cardiovascular disease (29). Given this remodeling at the ICD *in vivo*, we performed transmission electron microscopy of left ventricular myocardium at 12 wk post-AAV9 injection and observed a widening of the fascia adherens of the ICD in the CTNNA3-5A hearts (Fig. 7A). To further investigate remodeling of the cardiomyocyte adherens junction, immunofluorescence of

N-cadherin,  $\beta$ -catenin, and plakophilin 2 (PKP2) demonstrated significant internalization of all three proteins in the CTNNA3-5A hearts, with reduced fluorescent signal at the ICD, as compared to both empty and CTNNA3-WT tissues (Fig. 7B–D and SI Appendix, Fig. S19C–E). Moreover, correlation analysis between these proteins and CTNNA3-FLAG showed an increased colocalization with the CTNNA3-5A construct as compared to WT (Fig. 7B–D), suggesting that internalization of the unphosphorylatable protein also led to the internalization of its interacting partners at the adherens junction. Imaging of desmosome proteins, desmoplakin (DSP), and desmoglein (DSG), showed increased colocalization with FLAG and internalized protein expression in the CTNNA3-5A hearts for DSP, but not for DSG (SI Appendix, Fig. S19F–G), consistent with DSP acting as a closer interacting partner to CTNNA3 at the area composita between the adherens junction and the desmosome. To confirm the increased interaction with CTNNA3-5A, we lastly performed coimmunoprecipitation experiments. Analysis of total CTNNA3 in cardiac lysates and following FLAG immunoprecipitation confirmed CTNNA3 overexpression and enrichment (Fig. 7E). Immunoblotting for  $\beta$ -catenin following FLAG-pulldown and for CTNNA3 following N-cadherin-pulldown both demonstrated increased interaction with the CTNNA3-5A protein as compared to WT when normalized to input levels (Fig. 7E). Alternatively, immunoblotting for Cx43 following FLAG immunoprecipitation showed reduced interaction with the CTNNA3-5A protein as compared to CTNNA3-WT (Fig. 7E), supporting our



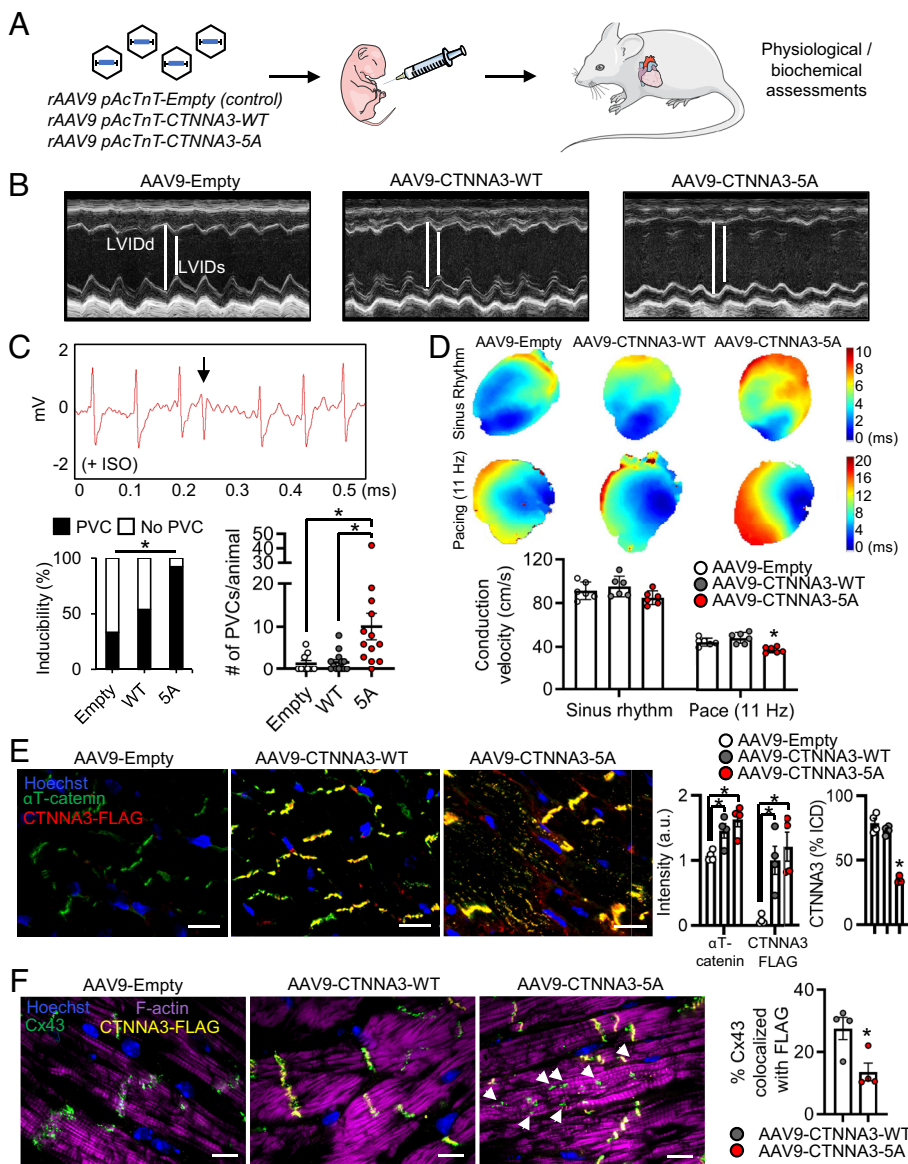


**Fig. 6.** In vivo overexpression of phosphonull CTNNA3 leads to left ventricular contractile dysfunction and electrical abnormalities. (A) Schematic illustration of mouse model of CTNNA3 phosphomutant overexpression. (B) Representative M-mode echocardiography recordings at 12 wk post-AAV9 injection. (C) Representative ECG recording of premature ventricular contraction (PVC; arrow) following isoproterenol administration. AAV9-CTNNA3-5A mice showed increased susceptibility to isoproterenol-induced PVCs over a continuous 30-min ECG recording following isoproterenol bolus (AAV9-Empty  $n = 9$ , AAV9-CTNNA3-WT  $n = 13$ , AAV9-CTNNA3-5A  $n = 13$ ).  $*P < 0.05$  by Fisher's exact test (inducibility) or by one-way ANOVA and Tukey post hoc test (# of PVCs/animal). (D) Representative isochronal activation maps of optically mapped (di-4-ANEPPS) isolated hearts at sinus rhythm (Top) and paced at 11 Hz from the left ventricular free wall (Middle) showing time to activation of the ventricle from the site of stimulation. Average conduction velocities of hearts in sinus rhythm or paced from the left ventricular free wall showed conduction slowing in AAV9-CTNNA3-5A hearts under pacing (Bottom).  $n = 6$  hearts/group.  $*P < 0.05$  vs. all other groups, by one-way ANOVA and Tukey post hoc test. (E) Confocal imaging of mouse myocardium stained for total  $\alpha$ T-catenin and CTNNA3-FLAG at 12 wk postinjection (Left) showed overexpression of total CTNNA3 and FLAG-tagged constructs (Middle), as well as internalization of the CTNNA3-5A protein (Right). (Scale bar, 20  $\mu$ m.)  $*P < 0.05$  by one-way ANOVA and Tukey post hoc test. (F) Confocal imaging of connexin 43 (Cx43), F-actin, and CTNNA3-FLAG in the heart at 12 wk postinjection (Left) showed internalization/lateralization (arrowheads) of Cx43 signal and reduced colocalization with FLAG (Right) in AAV9-CTNNA3-5A myocardium. (Scale bar, 10  $\mu$ m.) All images shown are representative of 10 fields of view per heart, from  $n = 4$  mice per group. See [S1 Appendix](#) for individual channel images.

imaging results of Cx43 internalization and dissociation from the adherens junction in the AAV9-CTNNA3-5A myocardium. Altogether, loss of CTNNA3 phosphorylation led to internalization of these protein complexes and dissociation from the ICD.

## Discussion

To better understand the heterogeneous nature of human HF, we used left ventricular tissue samples from patients with either DCM or ICM, including samples from the left ventricular infarct, peri-infarct, and noninfarct regions, to better represent the etiology- and region-specific sequelae of cardiac dysfunction. Previous phosphoproteomic studies in ischemic and nonischemic HF identified 782 total proteins, 823 total phosphopeptides, and 26 differential phosphoproteins (30), with a more recent in press dataset identifying 15,816 total phosphopeptides with 281 differential phosphoproteins between advanced DCM and NFC (14). Here, we identified and quantified 5,570 proteins with 13,624 phosphorylation sites corresponding to 3,240 phosphoproteins, of which 195 were uniquely altered in DCM and 809 uniquely altered in infarct-related regions of ICM patients. Each of our pair-wise comparisons, DCM and NFC, infarct and noninfarct, and periinfarct and noninfarct, revealed unique global proteomic

and phosphoproteomic profiles with both shared and disease-/region-specific perturbations.

Downstream bioinformatics analyses identified functional enrichment of cell-cell adhesion pathways in DCM, which interestingly has also been observed as an etiology-specific signature in other larger human DCM proteomic and transcriptomic datasets (14, 31). These analyses led us to highlight a DCM-associated hyperphosphorylation of the cardiomyocyte ICD protein,  $\alpha$ T-catenin (CTNNA3). Despite the limitations of a bulk tissue (phospho)proteomic workflow, we were able to demonstrate CTNNA3 as a cardiomyocyte-enriched candidate protein. Biological follow-up experiments using nonphosphorylatable or phosphomimetic constructs of CTNNA3 revealed internalization of the phosphonull protein in ex vivo lentiviral-transduced adult mouse cardiomyocytes and in vivo in intact mouse heart tissue sections following AAV9-mediated overexpression. Further in vivo analyses in mice revealed that overexpression of the phosphonull protein, but not the wildtype, led to adverse left ventricular remodeling, contractile dysfunction, and electrical conduction abnormalities. These changes were accompanied by remodeling of the ICD, including cointernalization of the phosphonull CTNNA3 with other proteins of the adherens junction/area composita, as well as well-established hallmarks of ICD disorganization, including gap junction dissociation (29) and widening of the fascia adherens (32).

**Table 2. Overexpression of phosphonull CTNNA3 leads to left ventricular dilation and contractile dysfunction determined by echocardiography**

	AAV9-empty	AAV9-CTN-NA3-WT	AAV9-CTN-NA3-5A
<i>n</i>	10	16	16
4 wk postinjection			
Body weight (g)	20.80 ± 0.61	20.94 ± 0.96	21.63 ± 1.02
LVEDV (μL)	42.74 ± 2.48	44.97 ± 1.97	48.08 ± 2.24
LVESV (μL)	18.35 ± 1.48	18.23 ± 0.86	18.26 ± 0.99
LVIDd (mm)	3.74 ± 0.07	3.74 ± 0.04	3.87 ± 0.06
LVIDs (mm)	2.33 ± 0.07	2.37 ± 0.04	2.58 ± 0.05 *
EF (%)	67.52 ± 0.96	67.23 ± 0.97	62.52 ± 1.10 §
FS (%)	36.92 ± 0.73	36.78 ± 0.77	33.34 ± 0.76 §
LVAWd (mm)	0.70 ± 0.01	0.75 ± 0.01	0.75 ± 0.01
LVAWs (mm)	1.03 ± 0.02	1.02 ± 0.03	0.98 ± 0.02
LVPWd (mm)	0.71 ± 0.01	0.70 ± 0.01	0.72 ± 0.01
LVPWs (mm)	1.12 ± 0.02	1.01 ± 0.03	1.01 ± 0.02
LV mass (mg)	89.74 ± 4.34	91.87 ± 2.67	99.78 ± 2.56
LV mass (corr) (mg)	71.79 ± 3.47	73.50 ± 2.14	79.82 ± 2.05
HR (bpm)	443 ± 13	464 ± 13	442 ± 11
8 wk postinjection			
Body weight (g)	25.60 ± 1.76	27.13 ± 0.97	29.00 ± 1.01
LVEDV (μL)	54.82 ± 3.04	53.38 ± 2.75	63.50 ± 3.01 §
LVESV (μL)	21.99 ± 1.54	21.27 ± 1.81	28.88 ± 1.86 *
LVIDd (mm)	3.92 ± 0.07	3.99 ± 0.06	4.21 ± 0.05 *
LVIDs (mm)	2.44 ± 0.08	2.60 ± 0.07	3.04 ± 0.07 **
EF (%)	68.30 ± 1.48	64.05 ± 1.24	53.90 ± 2.17 **
FS (%)	37.76 ± 1.17	34.57 ± 0.88	27.86 ± 1.37 **
LVAWd (mm)	0.79 ± 0.02	0.80 ± 0.01	0.81 ± 0.01
LVAWs (mm)	1.15 ± 0.03	1.07 ± 0.02	1.04 ± 0.02 #
LVPWd (mm)	0.76 ± 0.02	0.78 ± 0.01	0.79 ± 0.01
LVPWs (mm)	1.18 ± 0.05	1.15 ± 0.02	1.10 ± 0.02
LV mass (mg)	109.62 ± 5.96	114.93 ± 4.24	127.21 ± 4.10 #
LV mass (corr) (mg)	87.70 ± 4.77	91.95 ± 3.40	102.76 ± 2.91 #
HR (bpm)	430 ± 12	453 ± 13	427 ± 14
12 wk postinjection			
Body weight (g)	28.40 ± 1.94	29.94 ± 1.06	32.06 ± 1.16
LVEDV (μL)	54.58 ± 3.44	53.37 ± 1.85	66.49 ± 3.27 *
LVESV (μL)	21.81 ± 1.68	25.45 ± 1.68	30.14 ± 2.47 #
LVIDd (mm)	3.89 ± 0.07	4.01 ± 0.06	4.28 ± 0.06 *
LVIDs (mm)	2.47 ± 0.07	2.68 ± 0.06	3.17 ± 0.06 **
EF (%)	66.76 ± 1.42	62.07 ± 1.20	51.25 ± 1.17 **
FS (%)	36.53 ± 1.08	33.12 ± 0.85	26.05 ± 0.70 **
LVAWd (mm)	0.82 ± 0.01	0.84 ± 0.02	0.83 ± 0.01
LVAWs (mm)	1.19 ± 0.02	1.16 ± 0.03	1.09 ± 0.02 #
LVPWd (mm)	0.77 ± 0.01	0.81 ± 0.02	0.83 ± 0.02 #
LVPWs (mm)	1.20 ± 0.04	1.14 ± 0.02	1.16 ± 0.03
LV mass (mg)	111.81 ± 5.28	123.92 ± 5.31	138.06 ± 4.67 *
LV mass (corr) (mg)	89.45 ± 4.23	99.20 ± 4.27	110.37 ± 3.74 *
HR (bpm)	453 ± 10	434 ± 8	450 ± 16

LVEDV, left ventricular end-diastolic volume; LVESV, left ventricular end-systolic volume; LVIDd, left ventricular internal dimension at diastole; LVIDs, left ventricular internal dimension at systole; EF, ejection fraction; FS, fractional shortening; LVAWd, left ventricular anterior wall at end diastole; LVAWs, left ventricular anterior wall at end systole; LVPWd, left ventricular posterior wall at end diastole; LVPWs, left ventricular posterior wall at end systole; LV, left ventricle; HR, heart rate. AAV9-empty: three male, seven female; AAV9-CTNNA3-WT: nine male, seven female; AAV9-CTNNA3-5A: 11 male, five female. \**P* < 0.05 AAV9-CTNNA3-5A vs. all other groups, \*\**P* < 0.0001 AAV9-CTNNA3-5A vs. all other groups, #*P* < 0.05 AAV9-CTNNA3-5A vs. AAV9-empty, §*P* < 0.05 AAV9-CTNNA3-5A vs. AAV9-CTNNA3-WT, by two-way ANOVA and Tukey post hoc test. Values are mean ± SEM.

The ICD constitutes a highly specialized cell–cell adhesion structure mediating electrical and mechanical coupling between cardiomyocytes (25). Importantly, genetic ICD protein defects have been well-established to drive dilated, hypertrophic, and arrhythmogenic cardiomyopathies (25, 33). Indeed, we and others have previously shown that disruption of the ICD contributes to structural, functional, and electrical defects driving heart disease pathogenesis (34–36). We hypothesize that CTNNA3 phosphorylation in the human DCM hearts may be an adaptive response to maintain cardiomyocyte–cardiomyocyte adhesion and appropriate mechanical and electrical coupling under conditions of increased mechanical stress, as seen in the diseased myocardium (9). Previous studies have demonstrated that germline loss of αT-catenin results in a DCM phenotype by 3 mo of age, coupled with ICD remodeling of the area composita and gap junction (36), while cardiac-specific double knockout of αE- and αT-catenin leads to internalized N-cadherin expression in the cardiomyocyte and perturbed ICD maturation (37). These studies implicate a key role for the CTNNA3 protein in regulating ICD structure and function, however how phosphorylation can affect CTNNA3 protein function and localization has not been previously explored. All five putative phosphorylation sites investigated in this study are located within a conserved amino acid region within the CTNNA3 protein, termed the phospho (P)-linker domain (26). In support of our findings, nonphosphorylatable constructs in this domain of the closely related αE-catenin (CTNNA1) showed similar defects in intercellular adhesion (26). Moreover, deletion of the P-linker domain leads to internalized cytosolic expression of the CTNNA3 protein and loss of expression at cell–cell contacts (38). This is in line with our findings in both isolated cardiomyocytes and in intact myocardium in vivo demonstrating ICD remodeling and internalized expression of the unphosphorylatable protein construct within the cardiomyocyte. Interestingly, there is a documented human single-nucleotide variant at one of these phosphorylated residues, S650, resulting in a missense mutation from serine to asparagine that is associated with arrhythmogenic right ventricular cardiomyopathy (39), suggesting a potential clinical relevance of our αT-catenin phosphomutants. Ultimately, these data support the notion of DCM-associated changes at the ICD and reinforce the utility of phosphoproteomic analyses to characterize pathways in the pathogenesis of HF.

Several important limitations of our TMT multiplex-based workflow include the limited sample size of human patients in this analysis as well as the different comparisons between patients (i.e., DCM vs. NFC) and within patients (i.e., infarct vs. noninfarct regions). Our integrative analysis with open-access human datasets highlights the depth of coverage achieved in our approach and the conserved pathway level changes in disease at the global proteome level; however, it also highlights the variability across different patient cohorts in terms of individual differential protein expression in disease. Interestingly, the limited overlap of differentially expressed proteins in our integrated analysis is similar to other studies, with only 4% overlap observed in other literature comparisons of cardiac proteomic datasets (14). Moreover, access to healthy control tissues is always a limitation with studies using human cardiac tissue samples. In our study, non-failing control donors received pressor and inotropic support immediately prior to tissue explantation as standard clinical proceedings in the organ transplant program. Importantly, none of the DCM and ICM patients received inotropic support immediately prior to explantation of their native hearts. Moreover, our CTNNA3 findings in the human tissues showed increased phosphorylation in disease, supporting that this is not simply a result of vasopressor/inotrope-induced phosphorylation. Despite these limitations, to our knowledge, our

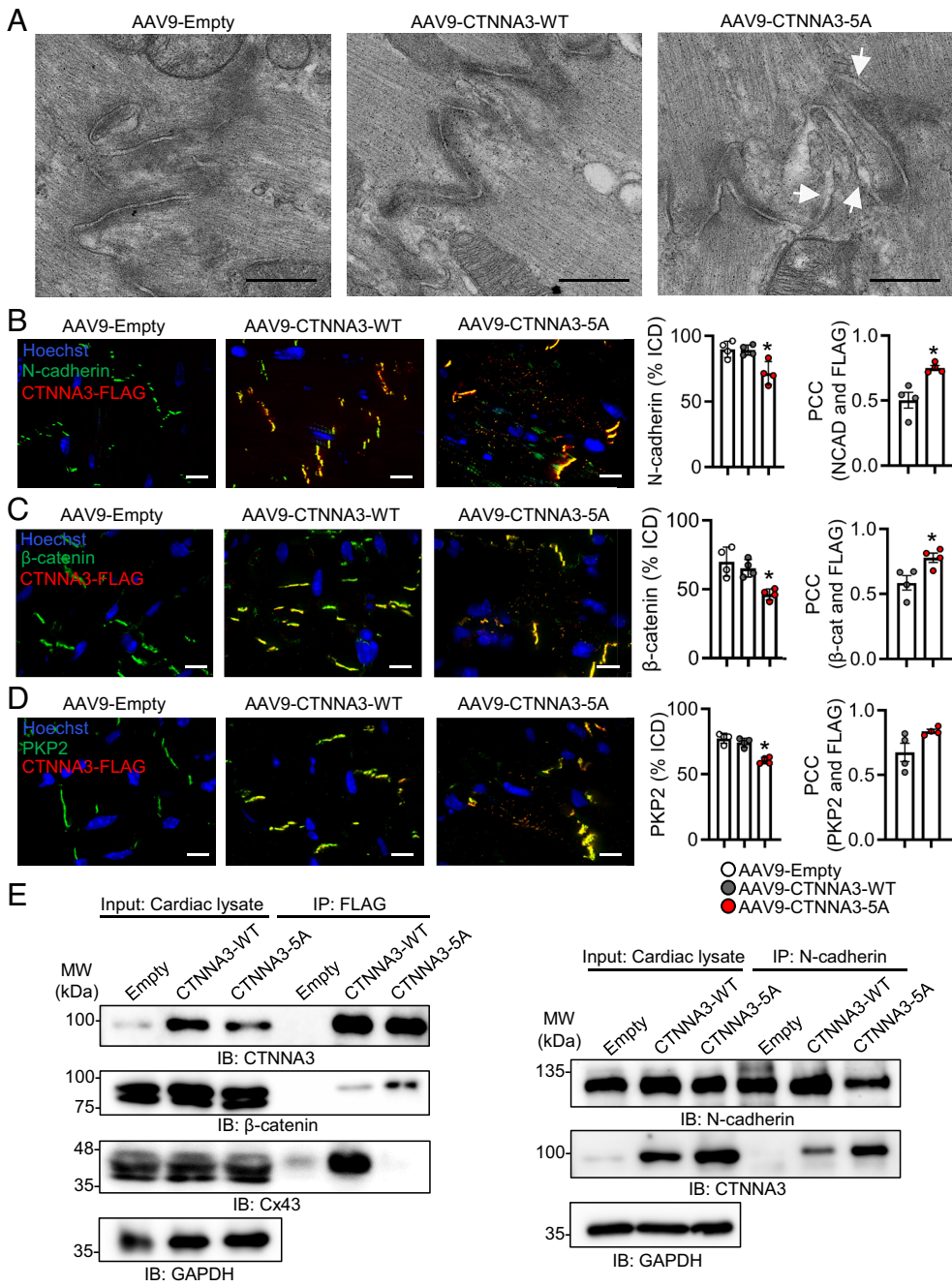


**Fig. 7.** Remodeling of the ICD in AAV9-CTNNA3-5A hearts. (A) Representative transmission electron microscopy of the ICD in hearts from mice 12 wk post-AAV9 injection. Widening of the fascia adherens (arrowheads) was found in AAV9-CTNNA3-5A hearts. Images taken at 28,000 $\times$  magnification. (Scale bar, 500 nm.) Confocal imaging of (B) N-cadherin, (C)  $\beta$ -catenin, and (D) plakophilin 2 (PKP2) in mouse myocardium at 12 wk post-AAV9 injection showed reduced percentage of the fluorescent signal at the ICD and colocalization with CTNNA3-FLAG by Pearson correlation coefficient (PCC). \* $P < 0.05$  by one-way ANOVA and Tukey post hoc test (% ICD) or by unpaired Student's  $t$  test (PCC). (Scale bar, 10  $\mu$ m.) All images shown are representative of 10 fields of view per heart, from  $n = 4$  mice per group. See *S1 Appendix* for individual channel images. (E) Co-immunoprecipitation assays using FLAG (Left) and N-cadherin (Right) showed overexpression and pull-down of the CTNNA3-FLAG construct in both AAV9-CTNNA3-WT and AAV9-CTNNA3-5A hearts, and interaction with  $\beta$ -catenin, connexin 43 (Cx43), and N-cadherin. Images are representative of at least  $n = 3$  independent biological replicates.

dataset provides the most detailed analysis of the cardiac phosphoproteome in human DCM and ICM to date, with many of these sites identified as of unknown biological significance. These phosphoproteomic data address the gap in knowledge to provide a detailed overview the key signaling cascades in HF.

Here, we provide a global network analysis and direct comparison of molecular signature perturbations at the protein and phosphorylation site level in DCM and region-specific ICM patients. We identify etiology-associated phosphorylation of CTNNA3 in DCM and demonstrate its importance as an adaptive mechanism to maintain the ultrastructural organization of the cardiomyocyte ICD, using both ex vivo and in vivo expression models. Strategies aimed at maintaining phosphorylation of CTNNA3 in hearts with DCM may slow the progression to end-stage HF state. Our study lays the groundwork for future phosphoproteomic profiling of the full spectrum of cardiac pathologies and provides rationale for direct subsequent detailed follow-up studies on individual signaling pathways

and molecular components involved in HF. Ultimately, these specific changes can be therapeutically targeted thereby elucidating a precision medicine-based approach to human HF.

## Materials and Methods

Adult nonfailing control and failing heart specimens were procured through the HOPE program (Human Organ Procurement and Exchange program, University of Alberta, Edmonton, Canada) and the Human Explanted Heart Program (HELP), as previously described (21, 40–42). This study was approved by the Institutional Review Committee/Human Research Ethics Board at the University of Alberta. Informed consent was obtained from all participants. All animal work was performed in accordance with the Canadian Council on Animal Care guidelines and approved by the University of Toronto Animal Care and Use Committee. A full description of experimental materials and methods for human heart sample preparation, histological analysis, tissue processing, (phospho)proteomic profiling and data analysis, animals, mouse tissue processing and cell culture,

immunoblotting, immunofluorescence, and molecular/biochemical assays is provided in *SI Appendix, Supplementary Materials and Methods*.

**Data, Materials, and Software Availability.** Mass spectrometry data have been deposited in ProteomeXchange (PXD012664) (43).

**ACKNOWLEDGMENTS.** We thank Dr. Jack Greenblatt, Dr. Edyta Marcon, and Mr. Hongbo Guo for assistance with mass spectrometry experiments, and Ms. Venus Chan for assistance with animal work. We thank Dr. Robert Hamilton and Ms. Meena Fatah for their help with the ECGenie system and Ms. Audrey Chong and Dr. Lindsey Fiddes for their assistance with electron microscopy. This research is part of the University of Toronto's Medicine by Design initiative which receives funding from the Canada First Research Excellence Fund. This work was funded by the Canadian Institutes of Health Research grants (PJT-153400) and Translational Biology and Engineering Program Ted Rogers

Centre for Heart Research seed grant to A.O.G. C.J.R. was supported by a CIHR Postdoctoral Fellowship. UK was supported by a Ted Rogers Centre Postdoctoral Fellowship.

Author affiliations: <sup>a</sup>Department of Physiology, Faculty of Medicine, University of Toronto, Toronto, ON M5S 1M8; <sup>b</sup>Translational Biology and Engineering Program, Ted Rogers Centre for Heart Research, Toronto, ON M5G 1M1; <sup>c</sup>Department of Medicine, University of Alberta, Edmonton, AB T6G 2R3; <sup>d</sup>Department of Biology, York University, Toronto, ON M3J 1P3; <sup>e</sup>Department of Biochemistry, Boston University School of Medicine, Boston, MA 02118; <sup>f</sup>Department of Biology, Boston University School of Medicine, Boston, MA 02118; <sup>g</sup>The Centre for Network Systems Biology, Boston University School of Medicine, Boston, MA 02118; and <sup>h</sup>Mazankowski Alberta Heart Institute, Edmonton, AB T6G 2B7

Author contributions: C.J.R., R.L., Y.-Q.Z., P.H.B., U.K., and A.O.G. designed research; C.J.R., M.T., D.H.K., S.S., R.L., A.C.T.T., Y.-Q.Z., W.L., S.H.-L., and U.K. performed research; C.J.R., M.T., S.S., G.Y.O., and U.K. contributed new reagents/analytic tools; C.J.R., M.T., D.H.K., S.S., R.L., A.C.T.T., Y.-Q.Z., S.H.-L., P.H.B., G.Y.O., U.K., and A.O.G. analyzed data; and C.J.R., M.T., S.S., R.L., A.C.T.T., A.E., G.Y.O., U.K., and A.O.G. wrote the paper.

1. G. B. o. D. S. Collaborators, Global, regional, and national incidence, prevalence, and years lived with disability for 301 acute and chronic diseases and injuries in 188 countries, 1990 to 2013: A systematic analysis for the global burden of disease study 2013. *Lancet* **386**, 743–800 (2015).
2. E. J. Benjamin *et al.*, Heart disease and stroke statistics-2017 update: A report from the American Heart Association. *Circulation* **135**, e146–e603 (2017).
3. C. Cook, G. Cole, P. Asaria, R. Jabbour, D. P. Francis, The annual global economic burden of heart failure. *Int. J. Cardiol.* **171**, 368–376 (2014).
4. A. P. Ambrosy *et al.*, The global health and economic burden of hospitalizations for heart failure: Lessons learned from the globalized heart failure registries. *J. Am. Coll. Cardiol.* **63**, 1123–1133 (2014).
5. D. Gajana *et al.*, Mortality in systolic heart failure revisited: Ischemic versus non-ischemic cardiomyopathy. *Int. J. Cardiol.* **224**, 15–17 (2016).
6. E. P. Tsagalou *et al.*, The long-term survival benefit conferred by intermittent dobutamine infusions and oral amiodarone is greater in patients with idiopathic dilated cardiomyopathy than with ischemic heart disease. *Int. J. Cardiol.* **108**, 244–250 (2006).
7. G. M. Felker *et al.*, Underlying causes and long-term survival in patients with initially unexplained cardiomyopathy. *N. Engl. J. Med.* **342**, 1077–1084 (2000).
8. E. M. McNally, L. Mestroni, Dilated cardiomyopathy: Genetic determinants and mechanisms. *Circ. Res.* **121**, 731–748 (2017).
9. J. S. Burchfield, M. Xie, J. A. Hill, Pathological ventricular remodeling: Mechanisms: part 1 of 2. *Circulation* **128**, 388–400 (2013).
10. S. H. Lee, D. H. Kim, U. Kuzmanov, A. O. Gramolini, Membrane proteomic profiling of the heart: Past, present, and future. *Am. J. Physiol. Heart Circ. Physiol.* **320**, H417–H423 (2021).
11. S. A. Michelhaugh, J. L. Januzzi Jr., Finding a needle in a haystack: Proteomics in heart failure. *JACC Basic Transl. Sci.* **5**, 1043–1053 (2020).
12. X. Yi, D. S. Jiang, G. Feng, X. J. Jiang, H. L. Zeng, An altered left ventricle protein profile in human ischemic cardiomyopathy revealed in comparative quantitative proteomics. *Kardiol. Pol.* **77**, 951–959 (2019).
13. D. Lu *et al.*, Cardiac proteome profiling in ischemic and dilated cardiomyopathy mouse models. *Front. Physiol.* **10**, 750 (2019).
14. S. G. Drakos *et al.*, Distinct transcriptomic and proteomic profile specifies patients who have heart failure with potential of myocardial recovery on mechanical unloading and circulatory support. *Circulation* **147**, 409–424 (2022), 10.1161/CIRCULATIONAHA.121.056600.
15. D. Dobrev, X. H. Wehrens, Role of RyR2 phosphorylation in heart failure and arrhythmias: Controversies around ryanodine receptor phosphorylation in cardiac disease. *Circ. Res.* **114**, 1311–1319 (2014).
16. B. Hudson, C. Hidalgo, C. Saripalli, H. Granzier, Hyperphosphorylation of mouse cardiac titin contributes to transverse aortic constriction-induced diastolic dysfunction. *Circ. Res.* **109**, 858–866 (2011).
17. J. Layland, R. J. Solaro, A. M. Shah, Regulation of cardiac contractile function by troponin I phosphorylation. *Cardiovasc. Res.* **66**, 12–21 (2005).
18. A. R. Marks, Calcium cycling proteins and heart failure: Mechanisms and therapeutics. *J. Clin. Invest.* **123**, 46–52 (2013).
19. M. Li *et al.*, Core functional nodes and sex-specific pathways in human ischaemic and dilated cardiomyopathy. *Nat. Commun.* **11**, 2843 (2020).
20. T. Tomin *et al.*, Mass spectrometry-based redox and protein profiling of failing human hearts. *Int. J. Omol. Sci.* **22**, 1787 (2021).
21. D. Reichart *et al.*, Pathogenic variants damage cell composition and single cell transcription in cardiomyopathies. *Science* **377**, eabo1984 (2022).
22. L. Jiang *et al.*, A quantitative proteome map of the human body. *Cell* **183**, 269–283.e219 (2020).
23. G. Y. Oudit *et al.*, Loss of PTEN attenuates the development of pathological hypertrophy and heart failure in response to biomechanical stress. *Cardiovasc. Res.* **78**, 505–514 (2008).
24. A. M. Samarel, Focal adhesion signaling in heart failure. *Pflugers Arch.* **466**, 1101–1111 (2014).
25. G. Zhao, Y. Qiu, H. M. Zhang, D. Yang, Intercalated discs: Cellular adhesion and signaling in heart health and diseases. *Heart Fail Rev.* **24**, 115–132 (2019).
26. D. J. Escobar *et al.*, alpha-Catenin phosphorylation promotes intercellular adhesion through a dual-kinase mechanism. *J. Cell Sci.* **128**, 1150–1165 (2015).
27. L. Wang *et al.*, Single-cell reconstruction of the adult human heart during heart failure and recovery reveals the cellular landscape underlying cardiac function. *Nat. Cell Biol.* **22**, 108–119 (2020).
28. A. Ortega *et al.*, Intercalated disc in failing hearts from patients with dilated cardiomyopathy: Its role in the depressed left ventricular function. *PLoS One* **12**, e0185062 (2017).
29. J. A. Palatinus, J. M. Rhett, R. G. Gourdie, The connexin43 carboxyl terminus and cardiac gap junction organization. *Biochim. Biophys. Acta* **1818**, 1831–1843 (2012).
30. M. A. Schechter *et al.*, Phosphoproteomic profiling of human myocardial tissues distinguishes ischemic from non-ischemic end stage heart failure. *PLoS One* **9**, e104157 (2014).
31. M. E. Sweet *et al.*, Transcriptome analysis of human heart failure reveals dysregulated cell adhesion in dilated cardiomyopathy and activated immune pathways in ischemic heart failure. *BMC Genom.* **19**, 812 (2018).
32. C. Basso *et al.*, Ultrastructural evidence of intercalated disc remodelling in arrhythmogenic right ventricular cardiomyopathy: An electron microscopy investigation on endomyocardial biopsies. *Eur. Heart J.* **27**, 1847–1854 (2006).
33. J. van Hengel *et al.*, Mutations in the area composita protein alphaT-catenin are associated with arrhythmogenic right ventricular cardiomyopathy. *Eur. Heart J.* **34**, 201–210 (2013).
34. A. C. T. Teng *et al.*, Tmem65 is critical for the structure and function of the intercalated discs in mouse hearts. *Nat. Commun.* **13**, 6166 (2022).
35. P. Sharma *et al.*, Evolutionarily conserved intercalated disc protein Tmem65 regulates cardiac conduction and connexin 43 function. *Nat. Commun.* **6**, 8391 (2015).
36. J. Li *et al.*, Loss of alphaT-catenin alters the hybrid adhering junctions in the heart and leads to dilated cardiomyopathy and ventricular arrhythmia following acute ischemia. *J. Cell Sci.* **125**, 1058–1067 (2012).
37. A. Vite, C. Zhang, R. Yi, S. Emms, G. L. Radice, alpha-Catenin-dependent cytoskeletal tension controls Yap activity in the heart. *Development* **145**, dev149823 (2018).
38. J. A. Heier *et al.*, Distinct intramolecular interactions regulate autoinhibition of vinculin binding in alphaT-catenin and alphaE-catenin. *J. Biol. Chem.* **296**, 100582 (2021).
39. National Center for Biotechnology Information, ClinVar; [VCV000409021.4]. <https://www.ncbi.nlm.nih.gov/clinvar/variation/VCV000409021.4>. Accessed 18 January 2023.
40. N. Parajuli *et al.*, Determinants of ventricular arrhythmias in human explanted hearts with dilated cardiomyopathy. *Eur. J. Clin. Invest.* **45**, 1286–1296 (2015).
41. S. Jana *et al.*, Disparate remodeling of the extracellular matrix and proteoglycans in failing pediatric versus adult hearts. *J. Am. Heart Assoc.* **7**, e010427 (2018).
42. V. B. Patel *et al.*, PI3Kalpha-regulated gelsolin activity is a critical determinant of cardiac cytoskeletal remodeling and heart disease. *Nat. Commun.* **9**, 5390 (2018).
43. U. Kuzmanov, A. O. Gramolini, PXD012664 - Integrative proteomic and phosphoproteomics analysis of human ischemic and dilated cardiomyopathic explant tissues identifies etiology-specific phosphorylation patterns and signaling pathways. ProteomeXchange Consortium. <https://proteomecentral.proteomexchange.org/cgi/GetDataset?ID=PXD012664>. Deposited 2 November 2019.